Journal of Visualization, Vol. 9, No. 3 (2006)265-274

Non-Contact 3D Flow-Structure Interaction Measurement (FSIM) System for Motion and Flow Fields

Interactions of a Vertical Cylinder Motion

Doh, D.H.*[1], Hwang, T.G.*[2], Jo, H.J.*[3], Pyeon, Y.B.*[4] Cho, Y.B.*[4] Tanaka, K.*[5] and Takei, M.*[6]

*1 Division of Mech. & Info. Eng., Korea Maritime University, Youngdo-ku, Busan, 606-791, Korea
Email: doh@mail.hhu.ac.kr
*2 Mech., Aerospace & Biomedical Eng. Dept, Univ. of Tennessee, Knoxville, U.S.A.
*3 Division of Ocean Systems Eng., Korea Maritime University, Youngdo-ku, Busan, Korea
*4 TNTech Co. Ltd., Busan, Korea
*5 Okamoto Co. Ltd., Tokyo, Japan
*6 Dept. of Mech. Eng., Nihon Univ., Tokyo 101-8308, Japan

Received 28 March 2005
Revised 11 February 2006

Abstract: A simultaneous measurement system that can analyze the flow-structure interactions has been developed. This system consists of four CCD cameras, two for capturing instantaneous flow fields and two for tracking a solid body. The three-dimensional vector fields around a cylinder are measured while the motion of the cylinder forced by the flow field is measured simultaneously with the constructed system. The cylinder is suspended in the circulating water channel and the surface of the working fluid is forced sinusoidal to make the cylinder bounced. Reynolds number for the mean main stream is about 3500. The interaction between the flow fields and the cylinder motion is examined quantitatively.

Keywords: 4-Camera, 3D-PTV, 6DOF-Motion, Flow-Structure Interactions (FSI).

1. Introduction

It is necessary to carry out analyses on the flow-structure interactions (FSI) of a floating vessel to evaluate its controllability and stability. For the analyses, numerical (or theoretical) and experimental approaches can be adopted.

With the help of recent rapid developments of computers, numerical approaches are widely adopted for the analyses. However, there are few research reports that can directly obtain the physical properties of the flow-structure interactions of floating vessels. Up to now, most of the analysis methods for the FSI have been using separate experimental data that were obtained through an independent experiment on the structure's motion and on the flow motion. For more accurate analysis on FSI, simultaneous measurement on the vessel's motion and its flow field is preferable.

As separate experimental methods for the FSI analysis, non-contact 6DOF(degree of freedom) motion measurement system (SRA, 1984) and non-contact three-dimensional PTV (3D-Particle Tracking Velocimetry) system (Doh et al., 2000) can be adopted. The former one is to measure the positions of the targets of the floating body based on the triangulation and the latter one is to measure the positions of numerous small particles of which densities are the same as that of the

working fluid by adopting the photogrammetry (Doh et al., 2002), and by introducing 3D-PTV algorithm (Doh et al., 2002) for the particles' pairing. Since the conventional 6DOF motion measurement system is based on a simple triangulation in which the lens distortion effect is neglected, the spatial resolution of the measured data is relatively large and the friction losses existed due to the LED system used as tracking targets. A revised system for 6DOF motion analysis that is complete non-contact has been commercialized recently. However, this system is expensive and does not measure the vector field of flows.

In this study, a new measurement system that can measure the 6DOF motion of floating body and its flow field simultaneously with complete non-contact is constructed by applying the 3D-PTVs carried out by Doh et al. (2002), Hagiwara et al. (2000) and Nishino et al. (1989). The 6DOF motion of a floating body is simultaneously measured with the 3D vector fields of the flows around the body.

2. Measurement System

2.1 Hardware and Measurement Procedures

Figure 1 shows the overall measurement system. Four CCD cameras (60 Hz, 512 x 512 pixels) were arranged as seen in the figure for simultaneous measurements of 6DOF motion of the floating body and its 3D flow field. Two cameras were used for the measurement of the motions of the four-targets installed on the floating body and the other two were used for the measurement of the 3D vector fields of the flow around the body. The floating body as shown in Fig. 2 and Fig. 3 (25 mm x 100 mm; D x H) was installed in a water channel (2500 mm x 300 mm x 80 mm; L x H x W). The hydrodynamic specification of the vertical-floating cylinder is shown on the Table 1. The water flow was circulated with the pump (0.5 kw) and a wave generator was installed on the surface of the upstream to produce waves onto this main stream. The Reynolds number is 3500 with the diameter of the vertical cylinder body.

The wave generator was operated with a motor (60 W) connected to the generator. The shape is of the quarter of a round cylinder (40 mm x 80mm; D x W) as seen in the figure. For non-contact measurements with the cameras, a camera calibration was carried out using two kinds of calibrators. One was used for the cameras for the 6DOF motion measurements and has 42 landmarks arranged 3-dimensionally on a table (80 mm x 110 mm x 10 mm; W x L x T). The machined spheres of 1 mm diameter were located at the tip of 0.5 mm diameter poles and they were painted with white. The positions of the small spheres (targets) were measured with an optical instrument (EG 2020CNC, precision = 1/1000 mm) in which a high-definition camera (2k x 2k) is installed onto the end of a high-precision traverse, and the images of the targets are magnified four times bigger than the originals to calculate exact centers of the targets. The other one was used for the cameras for the 3D-PTV measurements and has 100 grid points on a flat plate. After camera calibration was made, the main experiments were started with a working fluid seeded with nylon particles (φ = 250 μm, specific gravity = 1.02) circulated while operating the wave generator.

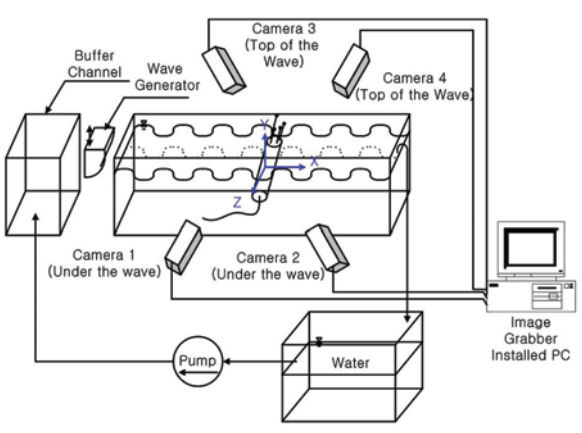

Fig. 1. Overall setup of the simultaneous measurement system.

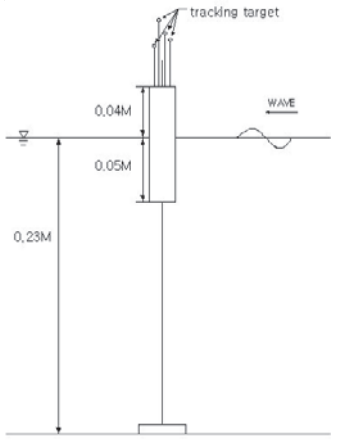

Fig. 2. Floating body configuration.

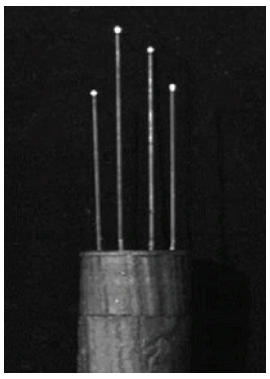

Fig. 3. The picture of the floating body.

Table 1. Specifications of the cylinder.

Draft	0.05 m
Center of Gravity	0.035 m
Weight	0.030 kgf
Displacement	0.114 kgf

The images of the four cameras were captured in simultaneous through an image grabber installed on the host computer (2 GHz). The centroids of the targets' image and the particles' image were used for the calculation of 6DOF motion of the floating body and of 3D vector field of the flows around the body.

2.2 Principle of Objects' 3D Tracking

In order to obtain the three-dimensional positional information of the targets of the floating body and the seeding particles of the flow field, their image centroids were used as photographic coordinates. These photographic coordinates and their absolute coordinates were used to calculate the parameters of the cameras.

In this study, 10 parameters (6 exterior parameters: $dis, \alpha, \beta, \gamma, m_x, m_y$, 4 interior parameters: c_x, c_y, k_1, k_2) were obtained. (α, β, γ) represents the tilting angles of the axes of the photographic coordinates against the absolute axes. Figure 4 shows a coordinate relation when the photographical axes had been set to parallel with the absolute coordinate by tilting with the angles (α, β, γ). (X, Y, Z) represents the absolute coordinate, and (x, y, z) the photographical coordinate of the image centroids of the targets and the seeded particles. The notation *dis* means the distance between the origin O(0, 0, 0) and the principal point (X_0, Y_0, Z_0) of the camera.

The coordinate (X_m, Y_m, Z_m) represents the position of the point P when the camera coordinate is rotated with the tilting angles to make the collinear equation on one line as shown in Fig. 4. The m_x, m_y means the point at which the normal vector from the origin O(Xo, Yo, Zo) of the camera coordinate meets with the X-Y plane. The collinear equation for every point between the two coordinates is expressed as Eq. (1). c_x and c_y are the focal distances for x and y components of the coordinate. Δx and Δy are the lens distortions as expressed as Eq. (2). The Eq. (1) can be converted to the following Eq. (3). Since this equation is a strong non-linear, an improved Gauss-Newton calculation method was adopted to obtain all necessary parameters using the above two equations in Eq. (3).

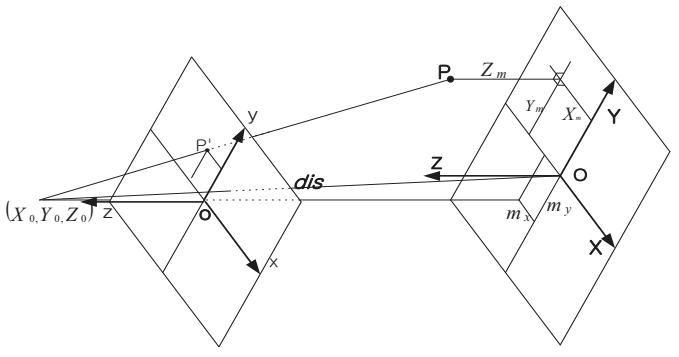

$$x = c_x \frac{Y_m - m_x}{\sqrt{dis^2 - m_x^2 - m_y^2} - Z_m} + \Delta x$$

$$y = c_y \frac{Y_m - m_y}{\sqrt{dis^2 - m_x^2 - m_y^2} - Z_m} + \Delta y \quad (1)$$

$$\Delta x = (x/r) \times \left(k_1 r^2 + k_2 r^4\right)$$
$$\Delta y = (x/r) \times \left(k_1 r^2 + k_2 r^4\right)$$
$$r = \sqrt{x^2 + y^2} \quad (2)$$

Fig. 4. Relations of camera parameters on the absolute coordinate and the photographical coordinate.

$$F = c_X \frac{X_m - m_X}{\sqrt{dis^2 - m_X^2 - m_y^2} - Z_m} - (x - \Delta x) = 0 \ , \quad G = c_y \frac{X_m - m_X}{\sqrt{dis^2 - m_X^2 - m_y^2} - Z_m} - (y - \Delta y) = 0 \tag{3}$$

Once all camera parameters are obtained, the relations between the photographic coordinate and the absolute coordinate of the targets' image or the particles' image can be expressed as the following Eq. (4).

$$\begin{bmatrix} X \\ Y \\ Z \end{bmatrix} = \mathrm{M}_M^{-1} \begin{bmatrix} X_m \\ Y_m \\ Z_m \end{bmatrix} = \mathrm{B} \begin{bmatrix} X_m \\ Y_m \\ Z_m \end{bmatrix} \tag{4}$$

Here, M_M is the matrix for the rotational transformation and B is its inverse matrix. (X_m, Y_m, Z_m) is expressed in the form of Eq. (5).

$$\mathrm{X}_m = \frac{x - \Delta x}{c_x} t + m_X \ , \ \mathrm{Y}_m = \frac{y - \Delta y}{c_y} t + m_y , \ \mathrm{Z}_m = \mathrm{d} - \mathrm{t}, \ \mathrm{d} = \sqrt{dis^2 - m_X^2 - m_y^2} \tag{5}$$

If the center of the camera is set to a vector (Xo, Yo, Zo), the collinear equation for one target (or particle) can be expressed as P(X, Y, Z) = (a_1 t + Xo, a_1 t + Yo, a_3 t + Zo). The cross-sectional points constructed from the following two collinear equations for the two cameras are defined as the three-dimensional positions in the absolute coordinate.

$$\mathrm{A(X, Y, Z)} = \mathrm{A}(a_{11}\,t + b_{11}, a_{12}\,t + b_{12}, a_{13}\,t + b_{13})$$

$$\mathrm{B(X, Y, Z)} = \mathrm{B}(a_{21}\,s + b_{21}, a_{22}\,s + b_{22}, a_{23}\,s + b_{23}) \tag{6}$$

Here, t and s are obtained by the least square method (LSM). Since the cross-sectional points do not always intersect on one point, the below Eq. (7) was used for the definition of the last three-dimensional position of the targets (or the particles), which stands for the midpoint of the shortest distance between the two collinear equations expressed as Eq. (6).

$$\begin{bmatrix} X_P \\ Y_P \\ Z_P \end{bmatrix} = \frac{1}{2} \left\{ \begin{bmatrix} X_A \\ Y_A \\ Z_A \end{bmatrix} + \begin{bmatrix} X_B \\ Y_B \\ Z_B \end{bmatrix} \right\} \tag{7}$$

Here, X_A, Y_A and Z_A represent the absolute coordinates for camera A defined by Eq. (6). X_B, Y_B and Z_B are for camera B.

Once the positions of the targets of the floating body and the particles around it have been obtained with the above method, the motion tracking and vector acquisition with temporal evolution are necessary to calculate the 6DOF motions and the 3D vector field. Figure 5 shows the concept of the motion tracking algorithm, "bidirectional tracking algorithm". In this algorithm, it is regarded that the same object between the two time image frames has been found on the condition that the original object's image (P_{11}) is seen in a certain area (Sr') of which center point is defined by the end point of the vector from the object P_{21} (dotted line from P_{21}) in the search area (Sr). In this study, Sr was set to 20 pixels and Sr' to 15 pixels. The algorithm for the acquisition of the 3D vector fields is the same used in the studies of Doh et al. (2004).

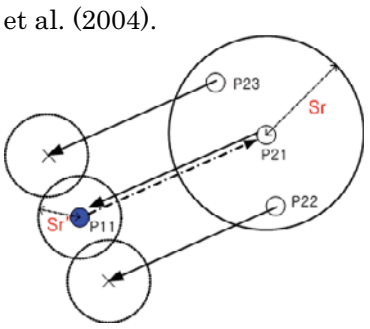

Fig. 5. Concept of the bidirectional tracking algorithm.

2.3 Validations of Measurement System

The performance of the 3D-PTV system adopted in this study can be referenced by the studies made by Doh et al. (2002, 2004). Accordingly, the performance test on the 6DOF-Motion system only is made. Figure 6 shows a picture of 6DOF-Motion system(Pusan National Univ.) used for the validation of the performance of the motion tracking system. Four targets were installed on the tracking system for motion tracking as shown in Fig. 7. Two cameras (500 Hz, 1k x 1k) were used for three-dimensional measurement. A plate (1.5 m x 1.5 m x 0.1 m) on which grid-type landmarks have been marked with white color with regular intervals as shown in Fig. 8 was used for camera calibration. This plate was traversed with a two-dimensional traversing machine. The images of the plate when traversed were used for camera calibration. Figure 9 shows the measurement results obtained by the 6DOF-Motion tracking system when the input commands were ordered for the motion system to produce surge and heave with 0.76 Hz. In Fig. 9 and others to be seen below, (x1, y1, z1) indicates measured three-dimensional positional data for the target number 1. Accordingly, (x2, y2, z2), (x3, y3, z3) and (x4, y4, z4) represent the data for the target number 2, 3, and 4, respectively. Table 2 shows a comparison table for the measurement results obtained by a commercial system and the measurement system constructed in this study. Figure 10 shows the definition of 6DOF. It can be seen that the measurement results by the system are relatively better than those by the commercial one. Since the results of the two systems were obtained in offline conditions separately, the comparisons on the phase lags between the two systems were not carried out. However, the differences of the amplitudes obtained by the two systems were within 1 % of the actual motions of which positions were commanded by the 6DOF-Motion system. In the mean time, a hybrid estimation for the measurement uncertainty of the system was carried out, in which the three-dimensional positional data of the calibrator were used as original reference data and the measured data were compared with these reference data. More than 20 measurements were carried out to get statistical data in which the discrepancies between the original data and the measured ones were evaluated. The average errors for x, y and z were 0.20 mm, 0.20 mm and 0.30 mm, respectively. And the variations for x, y and z were 0.30 mm, 0.25 mm and 0.55 mm, respectively. This indicates that the relative error was about 1 % for the measurement scales.

Fig. 6. 6DOF-Motion tracking system.

Fig. 7. Four targets installed on the 6DOF-Motion system.

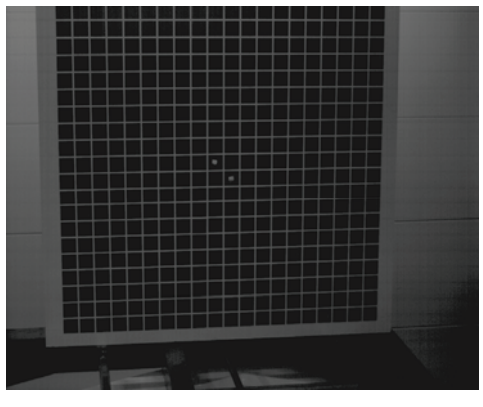

Fig. 8. Camera calibration plate.

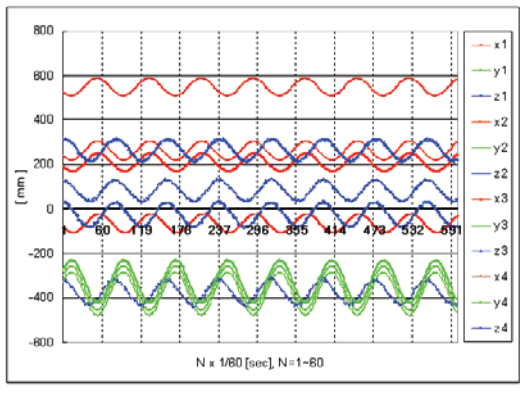

Fig. 9. Measured by the 6DOF-Motion tracking system.

Table 2. Comparison of measurement results.

Motion Mode	Input Freq. [Hz]	by Rodym DMM [Hz]	by present system [Hz]
Surge & Sway & Heave	0.760	0.750	0.756
Sway & Heave	0.900	0.892	0.896
Pitch	0.5	0.499	0.499
Surge	0.636	0.638	0.637
Heave	0.636	0.649	0.642
Sway	0.636	0.648	0.639

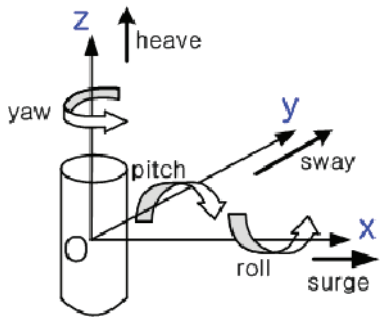

Fig. 10. Definition of 6 Degree-of-Freedom.

3. Application of the System to a Vertical Floating Cylinder

Figure 11(a) and Fig. 11(b) show the original images of the cameras 3 and 4 as seen in Fig. 1 for the four targets, and Fig. 12(a) and Fig. 12(b) show the images of the cameras 1 and 2 for the particles around the body. These four images were captured at the same time for simultaneous measurements. Using these consecutive images, calculation for 6DOF motion tracking and for 3D-PTV measurement is carried out following the ways mentioned in the previous sections. The magnitude of the sinusoidal wave motion of the wave generator was set to 2cm and the origin of the coordinate was set to (X, Y, Z: -150 mm, 0 mm, 0 mm) from the origin of the calibrator (0, 0, 0).

Figure 13, Fig. 14 and Fig. 15 show the measured results of the motion tracking of the four targets 1, 2, 3 and 4 when the wave generator was operated with 1 Hz, 1.33 Hz and 1.67 Hz, respectively. (x1, y1, z1) is the measured three-dimensional absolute coordinates of the target 1. It is seen from the figures that the measured x, y and z data for the four targets show similar modal wavy motions, which indicates that the measurement system can track the motion of the floating body reasonably. It can be said from the results on the three Figs. that the magnitudes of the objects' motion increase with the increase of wave frequencies. Further, it indicates that the natural frequency (resonance frequency) of the cylinder's motion is at higher frequency than 1.67 Hz. It is seen from Fig. 13 that the motion of z component, perpendicular to the wave's direction, becomes bigger at 1 Hz, and influences the pitching motion of the cylinder, which eventually makes the cylinder much more unstable. The second mode is seen on the vertical cylinder when the wave was operated with 1.33 Hz. It seems that the second mode is due to the nonlinear interactions between the heaving (y-axis motion) and the pitching motions of the cylinder while the motion of z component is becoming stable with periodical motion. It can be said from Fig. 15 that the primary mode of the x component of the cylinder motion is 1.6 Hz. This corresponds to the frequency of the wave generator, 1.67 Hz, which means that the motion of the cylinder is relatively stable and is governed by the wave propagation. It could be said from the whole experiment that the cylinder becomes very unstable when long periods of waves (lower frequencies) appeared. This is due to the vortex shedding and it generates a vertical motion onto the wave motions. Fig. 16 shows the profiles defined as the Eq. (8). This represents the average values of the whole absolute u and w vector components of the four targets at all frequencies. The decimal number 60 in the equation means the inverse value of the interval of the camera capture rate, 1/60 sec. This equation physically implies a degree of horizontal rotation. It seemed that the amplitudes of this motion become bigger and the repeating frequencies of the profile become lower with increase of wave frequencies, which indicates that the motions of sway and heave become stronger with increase of wave frequencies.

$$60 \cdot \left(\frac{1}{8}\right) \cdot \sum_{i=1}^{4} \left(|u_i| + |w_i|\right) \tag{8}$$

Figure 17(a) and Fig. 17(b) show instantaneous three-dimensional velocity vector fields around the floating body measured at the time of t = 25/60sec and t = 35/60sec. Figure 18(a) and Fig. 18(b) show the grid vectors (11 x 10 x 10) interpolated with the instantaneous random vectors of Fig. 17. It can be said from Fig. 18(a) and Fig. 18(b) that the flow motion made the floating body inclined at

(a) viewed by camera 3 (b) viewed by camera 4

Fig. 11. Original images of the four targets used for 6DOF motion tracking.

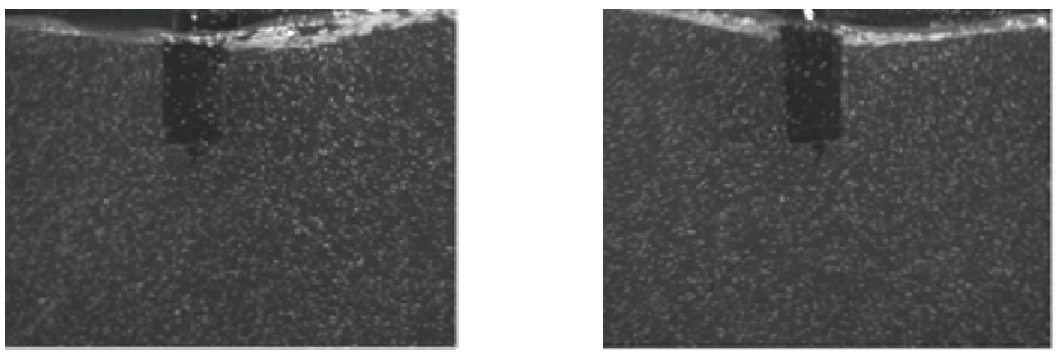

(a) viewed by camera 1 (b) viewed by camera 4

Fig. 12. Original images of the seeded particles used for 3D-PTV measurements.

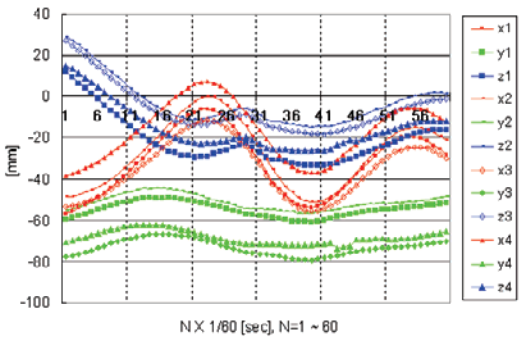

Fig. 13. Temporal motions of the four targets under the wave generator frequency 1 Hz.

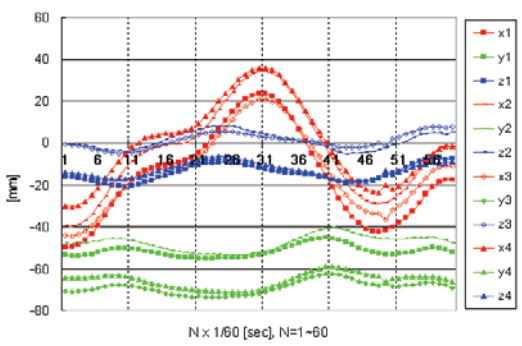

Fig. 14. Temporal motions of the four targets under the wave generator frequency 1.33 Hz.

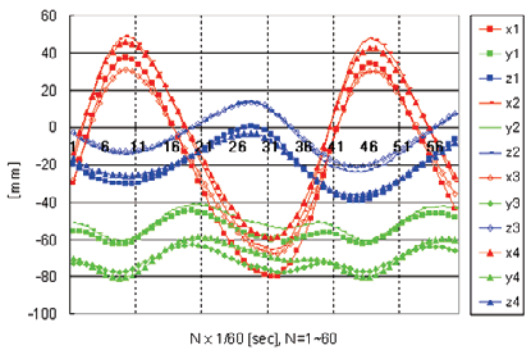

Fig. 15. Temporal motions of the four targets under the wave generator frequency 1.67 Hz.

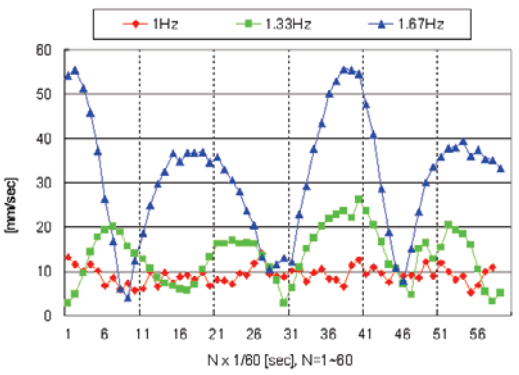

Fig. 16. Temporal characteristics of motions corresponding to the degree of rotation.

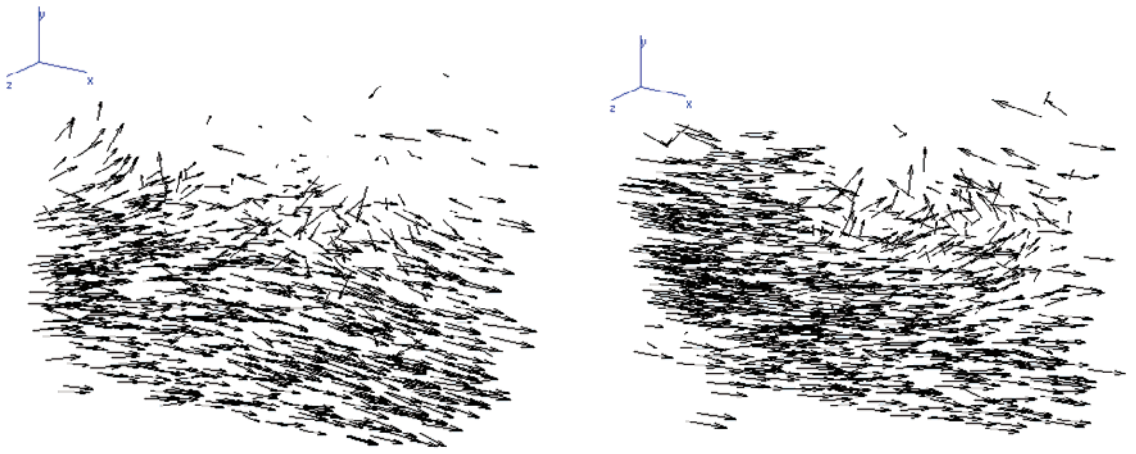

(a) t = 26/60 sec (b) t = 35/60 sec

Fig. 17. Instantaneous 3D vector field obtained by the constructed system.

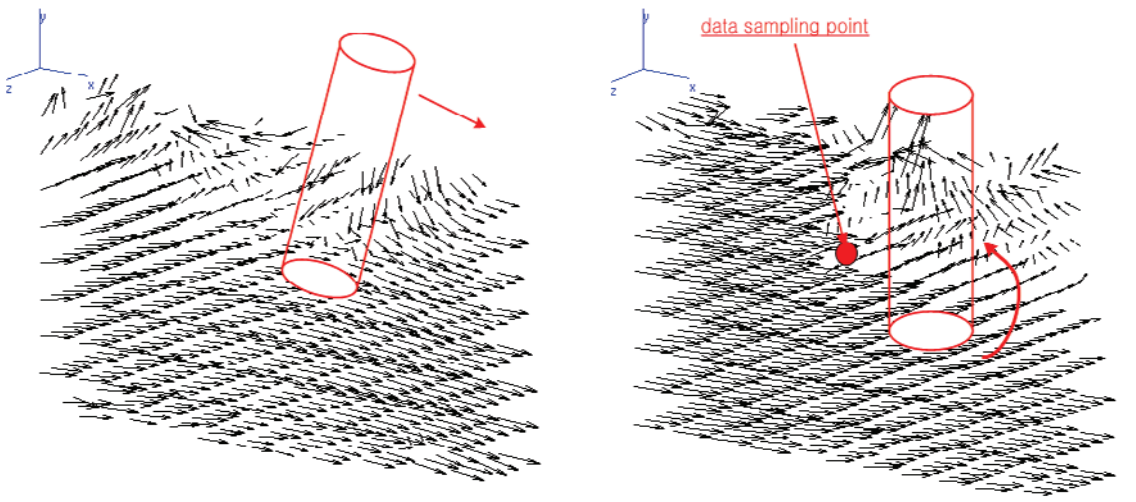

(a) t = 26/60 sec (b) t = 35/60 sec

Fig. 18. Instantaneous 3D vector fields on grids obtained by the constructed system.

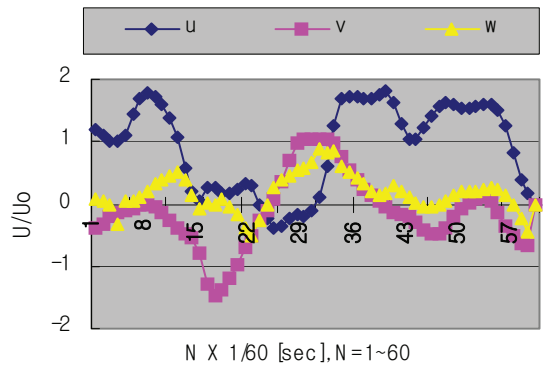

Fig. 19. Temporal evolutions of 3D vectors measured by 3D-PTV at x, y, z = (-20, -170, 0).

t = 25/60 sec to X direction (the arrow direction) and upright position at t = 35/60 sec. This is due to the fact that the wave coming from the upstream begins forcing the floating body at the time of t = 26/60 sec, which makes the body inclined and it is not inclined any more at the time of t = 35/60 sec because the wake generated from the bottom hits the body reversely at the time of t = 35/60 sec (see Fig. 18(b)). Figure 19 shows temporal evolutions of the velocity vector components measured by the constructed 3D-PTV system at the frequency of the wave generator 1.33 Hz. These were sampled at the position of (X, Y, Z) = (-20 mm, -170 mm, 0) from the calibration origin, which corresponds to the

position of X = -20 mm, Y = 15 mm and Z = 0 mm from the center point of the bottom plane of the floating cylinder (see Fig. 18(b)). It can be said that the frequency of U component is about 1.3 Hz though there is a second mode oscillation. In the mean time, the frequency of V component is about 1.9 Hz. The profile of W component is very complicate showing irregular frequencies. It seems that the floating body motion is strongly dependant on the U component (wave traveling direction). Interesting thing is that there exists a phase delay among the velocity components, from which the characteristics of the force from the fluid motion to the body can be estimated.

4. Conclusion

A new simultaneous measurement system for the 6DOF motion of a floating body and for the 3D flow field around the body has been successfully constructed. 6DOF-motion and 3D-flow fields of a floating vertical cylinder body were quantitatively obtained simultaneously.

Through a hybrid analysis on the measurement uncertainty, it is known that the average errors for X, Y and Z were 0.20 mm, 0.20 mm and 0.30 mm, respectively. And the variations for X, Y and Z were 0.30 mm, 0.25 mm and 0.55 mm, respectively. This indicates that the relative error was about 1 % for the measurement scales.

It was verified from the experiments that the frequency of the most conspicuous motion of the floating body to X-direction (U component) was the same as that of wave generator, which supports the system's reliability for motion measurements. The floating body motion is strongly dependant on the U component (wave traveling direction).

It seemed that the magnitudes of the horizontal and vertical motions of the body become larger when the wave frequency becomes bigger. The second mode was seen on the vertical floating cylinder when the wave was operated with 1.33 Hz. It is construed that the second mode is due to the nonlinear interactions between the heaving (Y-axis motion) and the pitching motions of the cylinder while the motion of Z component is becoming stable with periodical motion.

It has shown that the constructed system is useful for the analysis of flow-structure interactions (FSI) where issued.

Acknowledgements

The contents of the paper was carried out as parts of the research project (Singisul-Silyoung-Hwa Project, No.10008287) of Ministry of Commerce, Industry and Energy (ITEP) of Korea.

References

Doh, D. H., Kim, D. H., Choi, S. H., Hong, S. D., Kobayashi, T. and Saga, T., Single-frame 3-D PTV for High Speed Flows, Exp. in Fluids, 29-Suppl. (2000), 85-98.

Doh, D. H., Kim, D. H., Cho, K. R., Cho, Y. B., Saga, T. and Kobayashi, T., Development of GA based 3D-PTV Technique, Journal of Visualization, 5-3 (2002), 243-254.

Doh, D. H., Hwang, T. G. and Saga, T., 3D-PTV Measurements of the Wake of a Sphere, Measurement Science and Technology, 15-6 (2004), 1059-1066.

Hagiwara, Y., Nishino, M., Tanaka, M. and Sakamoto, S., 3-D PTV Measurement on Turbulence Modification Due to an Oil Droplet in a Plane Couette Water Flow, Journal of Visualization, 3-2 (2000), 101-114.

Nishino, K., Kasagi, N. and Hirata, M., Three-dimensional Particle Tracking Velocimetry Based on Automated Digital Image Processing. ASME J. Fluids Eng., 111-4 (1989), 384-391.

The Shipbuilding Research Association of Japan, A Study on the Load Forced on Floating Bodies and Its Restoring Characteristics, Research Reports 373 (1984).

Thompson, M. M., Manual of Photogrammetry, 4th Edition, American Society of Photogrammetry, (1980).

Author Profile

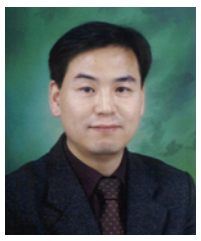

Deog Hee Doh: He received B.A. at Korea Maritime University (KMU) (1985). He finished his M.Sc. degree at the graduate school of KMU(1988). He received his PhD. degree at the Department of Mechanical Engineering of the University of Tokyo, Japan in 1995. His graduate works is on the development of 3D-PTV and simultaneous measurement techniques on temperature and velocity fields for thermal flows. He worked as an invited researcher for the Advanced Fluid Engineering Research Center (AFERC) in 1995. He has been working for Korea Maritime University since 1995 at the Division of Mechanical and Information Engineering. His research interests are to develop spatial measurement techniques such as 3D-PIVs, 3D-PTVs for nano-/bio- flows.

Tae Gyu Hwang : He received B.A. at Korea Maritime University (KMU) in 2001. He finished his M.Sc. degree at KMU in 2003. He received Ph.D. degree at the Department of Mechanical Engineering of KMU in 2005. His recent research area is on the near wake of a sphere using 3D PTV and on an impinging jet flow using 4D-PTV technique. His research interests are thermal flow visualization using 3D-PIV, 3D-PTV and micro PIV techniques.

Hyo Jae Jo: He received B.A. at Pusan National University (PNU) (1980). He finished his M.Sc. degree at the graduate school of PNU(1983). He received his PhD. degree at the Department of Ship and Ocean Engineering of the University of Tokyo, Japan in 1991. His graduate works is on the behaviour of offshore floating structure in the multi-directional waves. He worked as a visiting professor at Texas A&M University and researched a PIV technique in 2003. He has been working for Korea Maritime University since 1995 at the School of Ocean System Engineering. His research subjects are to simulate motions of floating structure in the oceans and to experiment at the basin for the flow visualization on the complex ocean environment.

Yong Beom Pyeon : He received B.A. at Korea Maritime University (KMU) in 2000. He finished his M.Sc. degree at KMU in 2003. He is a Ph.D. candidate of Mechanical Engineering at KMU since 2002 and is working at the development section of TNTech Co. Ltd. His recent research area is on the high speed air flows. His research interests are dynamic PIV analyses for bio-/nano-/micro- fluids.

Yong Bum Cho : He received B.A. at Korea Maritime University (KMU) in 2000. He finished his M.Sc. degree at KMU in 2003. He is a Ph.D. candidate of Mechanical Engineering at KMU since 2002 and is working at the development section of TNTech Co. Ltd. His recent research area is on the development of new codes that are applicable to the areas of the bio-/nano-/micro- fluid flows.

Kenji Tanaka: He received his Bachelor degree in Mechanical Engineering in 1986 from Nihon University, Tokyo Japan. He also received his M.Sc.(Eng.) degree in Mechanical Engineering in 1995 from Nihon University. He has been working for Okamoto Industries, INC. since 1986. His current position is a manager of cooperate administration. His research interests are Pneumatic conveying and PIV.

Masahiro Takei: He received his M.Sc.(Eng) in Resource Engineering in 1991 from Waseda University, Tokyo Japan. He also received his Ph.D. in Resource Engineering in 1995 from Waseda University. He has worked in Department of Mechanical Engineering, Nihon University, Tokyo Japan as an associate professor since 1995. His research interests are Computed tomography, Multiphase flow, Image processing and PIV.